International Journal of Computational Fluid Dynamics

ISSN: 1061-8562 (Print) 1029-0257 (Online) Journal homepage: http://china.tandfonline.com/loi/gcfd20

Resolution-optimised nonlinear scheme for secondary derivatives

Li Li, Changping Yu, Zhe Chen & Xinliang Li

To cite this article: Li Li, Changping Yu, Zhe Chen & Xinliang Li (2016) Resolution-optimised nonlinear scheme for secondary derivatives, International Journal of Computational Fluid Dynamics, 30:2, 107-119, DOI: 10.1080/10618562.2016.1164849

To link to this article: http://dx.doi.org/10.1080/10618562.2016.1164849

INTERNATIONAL JOURNAL OF COMPUTATIONAL FLUID DYNAMICS, 2016
VOL. 30, NO. 2, 107–119
http://dx.doi.org/10.1080/10618562.2016.1164849

Taylor & Francis
Taylor & Francis Group

Resolution-optimised nonlinear scheme for secondary derivatives

Li Li, Changping Yu, Zhe Chen and Xinliang Li

Institute of Mechanics, Chinese Academy of Sciences, Beijing, China

A 5-point-stencil optimised nonlinear scheme with spectral-like resolution within the whole wave number range for secondary derivatives is devised. The proposed scheme can compensate for the dissipation deficiency of traditional linear schemes and suppress the spurious energy accumulation that occurs at high wave numbers, both of which are frequently encountered in large eddy simulation. The new scheme is composed of a linear fourth-order central scheme term and an artificial viscosity term. These two terms are connected by a nonlinear weight. The proposed nonlinear weight is designed based on Fourier analysis, rather than Taylor analysis, to guarantee a spectral-like resolution. Moreover, the accuracy is not affected by the optimisation, and the new scheme reaches fourth-order accuracy. The new scheme is tested numerically using the one-dimensional diffusion problem, one-dimensional steady viscous Burger's shock, two-dimensional vortex decaying, three-dimensional isotropic decaying turbulence and fully developed turbulent channel flow. All the tests confirm that the new scheme has spectral-like resolution and can improve the accuracy of the energy spectrum, dissipation rate and high-order statistics of turbulent flows.

ARTICLE HISTORY
Received 10 July 2015
Accepted 5 March 2016

KEYWORDS
Spectral-like schemes; secondary derivatives; viscous terms; nonlinear optimisation; nonlinear weight

1. Introduction

High-resolution numerical schemes are widely used in detailed simulations of complex flows, such as direct numerical simulation (DNS) (Martín et al. 2006; Li, Fu, and Ma 2010) or large eddy simulation (LES) (Nagarajan, Lele, and Ferziger 2003; Sayadi and Moin 2012; Yu et al. 2013) of turbulent flows. In high-resolution simulations, all derivative terms of the Navier–Stokes equations, including both the first and the secondary derivatives, should be discretised using high-order numerical schemes. Most research efforts are directed towards the numerical methods for the first derivatives in the convection terms (Fu and Ma 1997; Yanwen et al. 1999; Deng and Zhang 2000; De and Eswaran 2006; Liang et al. 2009; Pirozzoli 2011; Tian and Yu 2011; Tian, Liang, and Yu 2011; Deng et al. 2012; Qin, Xia, and Tian 2014). According to Mattsson, Svärd, and Shoeybi (2008), the scheme of secondary derivatives may affect the stability of the calculation. The results of Suzuki et al. (2013) showed that the accuracy of high-order statistics can be increased by using higher order schemes of viscous terms. In LES, where central schemes are usually used for convective terms, the viscous terms are responsible for the stability of the calculation. Thus, numerical schemes for the secondary derivatives must be studied in-depth.

Compared with those on the first derivatives, works on the secondary derivatives are not sufficient. Lele (1992) summarised the general form of compact schemes and a method to optimise the schemes. Mohammadian (2010) compared the Fourier properties of two schemes for viscous terms in shallow flows. It was found that a proper treatment of the viscous terms could avoid the oscillations of the shortest resolvable waves. Shen, Zha, and Chen (2009), Shen and Zha (2010), Zingg et al. (2000) and Gerolymos and Vallet (2012) improved the resolution of the scheme of secondary derivatives with variable viscosity by reducing the stencil of the scheme. They obtained schemes in conservative forms, which were suitable for flows with shock waves. Mattsson, Svärd, and Shoeybi (2008) and Mattsson (2012) suggested the improvement of the resolution and stability of secondary derivatives using narrow stencils and also proposed boundary schemes with the summation-by-part (SBP) property. The resulting schemes were able to capture a weak viscous shock without any artificial viscosity. Vaassen, Vigneron, and Essers (2008) proposed a conservative and consistent scheme for viscous terms that possessed good accuracy, even for highly distorted unstructured meshes. Tu, Deng, and Mao (2011) proposed a staggered cell-edge high-order compact scheme, which can avoid the oscillations caused by cell-node high-order schemes. The works described above demonstrate that increasing the resolution of viscous terms helps suppress non-physical oscillations and stabilise the calculation.

CONTACT Xinliang Li lixl@imech.ac.cn

In LES, numerical errors are more evident than those in DNS because of the limited grid resolution (Chow and Moin 2003). Energy accumulation will occur within a high wave number range introduced by the aliasing errors of convective terms (Kennedy and Gruber 2008). Therefore, the performance of the schemes for viscous terms at high wave number is highly significant. High-resolution schemes of viscous terms are required to suppress this energy accumulation. However, high-resolution linear schemes, which are widely used in LES, always require large stencils. Wide stencils of computational points will reduce the parallel efficiency and restrict the application to problems with complex boundary conditions. This becomes an issue when designing a linear scheme with a short stencil and high resolution. In this paper, we abandon the linear framework and design a nonlinear scheme with both higher resolution and reduced stencil.

The most serious challenge in designing a nonlinear scheme is the nonlinear weight. A nonlinear scheme often comprises several linear schemes combined by nonlinear weights, such as the WENO (weighted essentially non-oscillatory) schemes (Jiang and Shu 1996). The form of the nonlinear weights is extremely important for a nonlinear scheme. Various shock sensors, limiters and nonlinear weights exist (Ducros et al. 1999; Harten 1978; Borges et al. 2008; Jameson et al. 1981; Ren, Liu, and Zhang 2003). However, they were specifically devised for discontinuity. In shock-free region, central schemes or compact schemes with little numerical dissipation are usually used for convective terms. The dissipation is mainly controlled by secondary derivatives. So, a new weight for shock-free region to control the dissipation of secondary derivatives is needed. In our work, we propose a new weight specifically designed for smooth flows based on Fourier analysis, considering that smooth flows can be expanded into Fourier series. Then the new weight will be applied in the design of a nonlinear scheme with a 5-point-stencil for secondary derivatives.

The paper is organised as follows, In Section 2, we show the shortages of linear optimisation in short stencils, such as low resolution and the overestimation of dissipation at low wave number; in Section 3, a new weight designed especially for smooth flows is proposed, and a spectral-like nonlinear scheme with a 5-point stencil is developed using the new weight; numerical tests of the one-dimensional (1D) diffusion problem, 1D steady viscous Burger's shock problem, 2D vortex diffusion problem, and 3D homogeneous isotropic decaying turbulence and fully developed turbulent channel flow are presented in Section 4 to verify the high resolution of the new scheme.

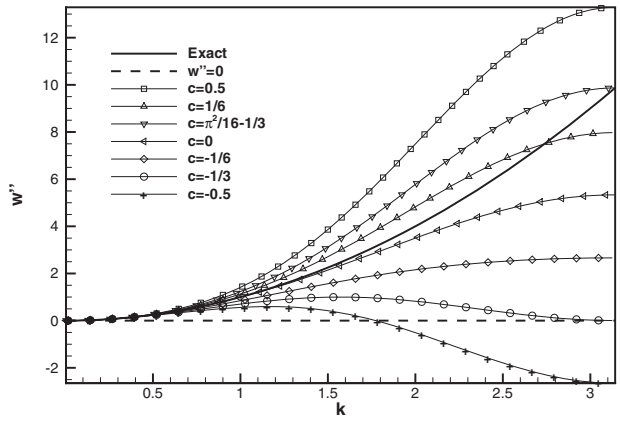

Figure 1. Plot of the Fourier property of the linear optimised schemes with different c's. The solid line represents the exact value of the reduced wave number. The dashed line represents $\omega'' = 0$. The other lines with symbols are the reduced numbers of linear schemes with different c's, from −0.5 to 0.5.

2. Analysis of the deficiency of linear optimisation

We restrict the scheme in a 5-point stencil for convenient application to complex geometries. Then the 5-point-stencil scheme for secondary derivatives can be written in the following form:

$$\frac{\partial^2 u}{\partial x^2} = \frac{-\left(u_{i+2}+u_{i-2}\right)+16\left(u_{i+1}+u_{i-1}\right)-30u_i}{12\Delta x^2} - c\frac{\left(u_{i+2}+u_{i-2}\right)-4\left(u_{i+1}+u_{i-1}\right)+6u_i}{\Delta x^2} \quad (1)$$

where the first term of the right-hand terms is a standard fourth-order central scheme and the second term is a second-order artificial dissipation term.

Suppose $u = \exp(ikx)$. Then, the exact value of $\frac{\partial^2 u}{\partial x^2}$ is $-k^2\exp(ikx)$. Substituting $u = \exp(ikx)$ into the scheme above, we obtain $\frac{\partial^2 u}{\partial x^2} = -w''\exp(ikx)/\Delta x^2$. w'' is called the reduced wave number, and w'' of the scheme is as follows:

$$w''(\alpha) = \left[2\cos(2\alpha) - 32\cos(\alpha) + 30\right]/12 + c\left[2\cos(2\alpha) - 8\cos(\alpha) + 6\right] \quad (2)$$

where $\alpha = k\Delta x$ is the scaled wave number, which ranges from 0 to π.

The exact value of w'' is α^2. The scheme underestimates the dissipation if $w'' < \alpha^2$ and overestimates the dissipation if $w'' > \alpha^2$. The w'''s for different $c's$ are shown in Figure 1. It is illustrated that $w'' \le \alpha^2$ on the condition that $c \le 0$, which means that the scheme underestimates dissipation at all wave numbers. We note that $c = 0$ represents the standard fourth-order scheme. On condition that the discretisation of convective terms produces no

numerical errors, standard central schemes will lead to entropy deficiency. Only if $c \geq \frac{\pi^2}{16} - \frac{1}{3}$ is chosen can the scheme produce sufficient entropy over the whole wave number range. However, it is too dissipative at high wave numbers. The overestimated viscosity will reduce the resolution and dampen the useful information of fine-scale structures. Therefore, a perfect scheme with both stability and high resolution is difficult to develop in the form of Equation (1). We will resort to the nonlinear correction to modify the scheme in the next part.

3. Nonlinear scheme for secondary derivatives

The key point of nonlinear optimisation is to add adaptive artificial dissipation to the standard fourth-order scheme. As seen in Figure 1, the dissipation deficiency of the fourth-order central scheme is small at low wave numbers and large at high wave numbers. Therefore, the artificial dissipation is designed to be small at low wave numbers and relatively large at high wave numbers. We write the nonlinear scheme in the following form:

$$\frac{\partial^2 u}{\partial x^2} = \frac{-(u_{i+2}+u_{i-2})+16(u_{i+1}+u_{i-1})-30u_i}{12\Delta x^2} - c(u_{i-2},\ldots,u_{i+2}) \times \frac{(u_{i+2}+u_{i-2})-4(u_{i+1}+u_{i-1})+6u_i}{\Delta x^2} \quad (3)$$

where c is a function of u instead of being a constant, as in Section 2. A proper form of c should be designed to ensure that the modified wave number is similar to the exact solution. c is rewritten in the form $c = c_0\hat{\theta}_j$, where $\hat{\theta}_j$ is a nonlinear weight ranging from 0 to 1. If the coefficient c_0 is set to $\frac{\pi^2}{16} - \frac{1}{3}$, the nonlinear weight should take the value of zero at $\alpha = 0$ and 1 at $\alpha = \pi$ to ensure that w'' is exact at $\alpha = 0$ and $\alpha = \pi$. Moreover, $\hat{\theta}_j$ should be a monotonous function of α to add more viscosity at high wave numbers and less at low wave numbers. Then, the main task is to design $\hat{\theta}_j$.

3.1. Design of a nonlinear weight based on Fourier analysis

Unlike shock sensors, which aim to identify discontinuity (i.e., shock or contact discontinuity), $\hat{\theta}_j$ aims to recognise high-frequency waves in smooth flows. This motivates us to search for a nonlinear weight with good properties in Fourier space.

A good nonlinear weight in Fourier space should have the following properties:

(1) The value of the weight should be constant for a single cosine/sine wave at a certain wave number α.

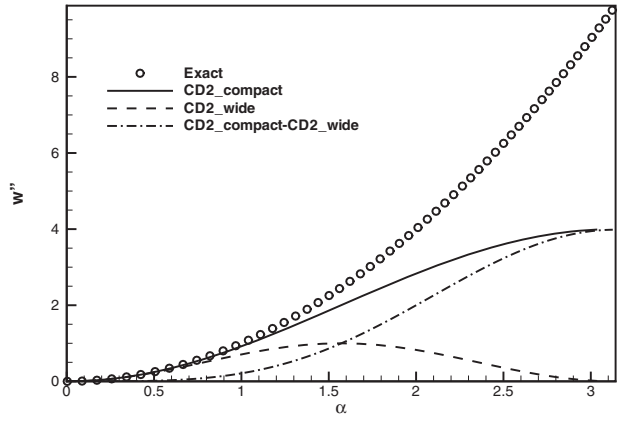

Figure 2. Plot of the Fourier property of schemes CD2_compact and CD2_wide. The solid and dashed lines are the reduced wave numbers of CD4 and OCD4, respectively. The dash–dot line is the difference between the two schemes.

(2) It should be a smooth and monotone function of the wave number.

(3) It should take the value of 0 at $\alpha = 0$ and 1 at $\alpha = \pi$.

First, we follow the design philosophy of Harten's sensor and write the new weight in the following form:

$$\hat{\theta}_j = \left| \frac{|S_1| - |S_2|}{|S_1| + |S_2|} \right| \quad (4)$$

$S_1 = u_{j+1} - u_j$ and $S_2 = u_j - u_{j-1}$ are selected in Harten's sensor, assuming that $|u_{j+1} - u_j| - |u_j - u_{j-1}|$ is of the order of $O(\Delta x^2)$ in smooth flow and $O(1)$ near a shock. Thus, the value of the switch is small in smooth flow and 1 near a shock.

Now, we change the order analysis to Fourier analysis. A new S_1 and S_2 should be designed with the property that $|S_1| - |S_2| \sim O(\alpha^n)$ at low wave numbers and $|S_1| - |S_2| \sim O(1)$ at high wave numbers, where $\alpha = k\Delta x$.

Here, we propose a simple design. First, we observe the dissipative property of the following schemes: CD2_compact and CD2_wide

$$\text{CD2\_compact}: u'' = (u_{i+1} + u_{i-1} - 2u_i)/\Delta x^2 \quad (5)$$

$$\text{CD2\_wide}: u'' = (u_{i+2} + u_{i-2} - 2u_i)/\left(4\Delta x^2\right) \quad (6)$$

As shown in Figure 2, the dissipation of the scheme with a wide stencil tends towards zero at $\alpha = \pi$, while that with a compact stencil tends towards a non-zero positive value. The difference between the two schemes increases as the wave number increases. This property can be used to construct a weight coefficient, as follows:

$$S_1 = |u_{i+1} + u_{i-1} - 2u_i| \quad (7)$$

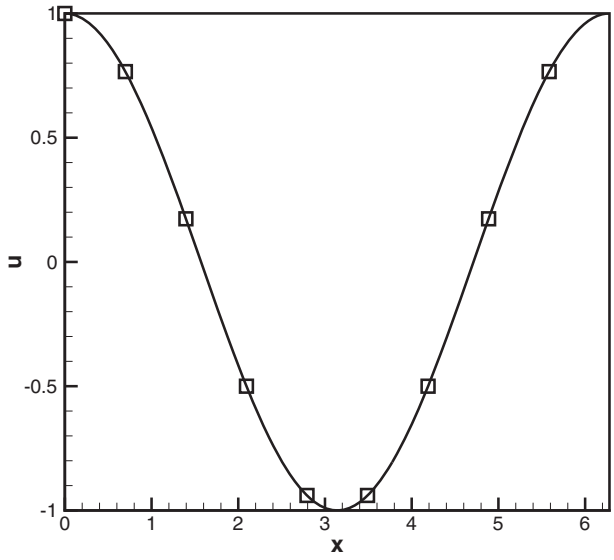

Figure 3. Plot of a cosine wave and the discrete points on it.

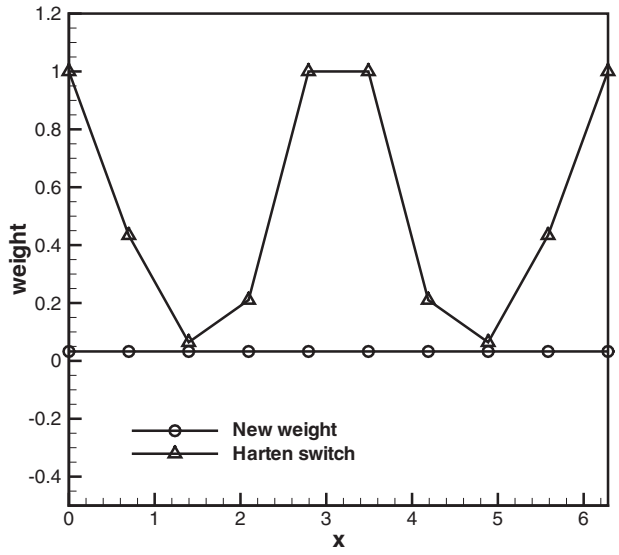

Figure 4. The value of different nonlinear weights at different points. The solid line with circles represents the value of the new weight, and the solid line with triangles represents the value of Harten switch.

$$S_2 = |u_{i+2} + u_{i-2} - 2u_i| / 4 \tag{8}$$

$$\hat{\theta}_j = \left|S_1^r - S_2^r\right| / \left|S_1^r + S_2^r\right| \tag{9}$$

$\hat{\theta}_j$ is constructed by scheme CD2_compact and scheme CD2_wide. These two schemes produce similar results at low wave numbers but are very different at high wave numbers. Thus, the weight coefficient $\hat{\theta}_j$ tends towards 0 at low wave numbers and approaches 1 at high wave numbers monotonously. Moreover, we can also verify that the new weight is independent of the physical positions for a single cosine/sine wave. We take the cosine wave as an example. The value of the new weight for a cosine wave is as follows:

$$S_1 = |2\cos(\alpha) - 2|\,|\cos(kx)| \tag{10}$$

$$S_2 = |2\cos(2\alpha) - 2|\,|\cos(kx)| / 4 \tag{11}$$

$$\hat{\theta}_j = \left|S_1^r - S_2^r\right| / \left|S_1^r + S_2^r\right| \tag{12}$$

It is easy to see that the only term relative to x, i.e., $|\cos(kx)|$, will disappear as a result of division. Then, the resulting weight is a simple function of α, which satisfies all the requirements mentioned above. Note that there is an adjustable coefficient r in $\hat{\theta}_j$. We should optimise the r to match the spectral property.

Figure 4 presents an example in which we discretise a cosine wave (see Figure 3) with 10 points, namely $\alpha = \pi/9$. The values of the Harten switch and the new sensor ($r = 2$ is given) at different nodes are given. It can be seen that the new weight takes the same value at all points,

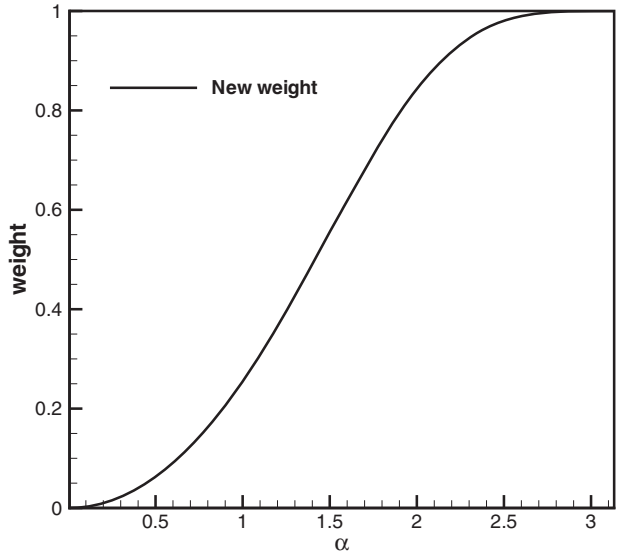

Figure 5. The value of the new weight versus α.

which is the desired result. Figure 5 shows the value of the weight versus α. The properties of the weight in Fourier space satisfy all the requirements mentioned above.

Taylor analysis of the nonlinear weight shows that

$$\hat{\theta}_j \sim (r-2)(r-3)\Delta x^2$$

If $r \neq 2$ and $r \neq 3$, then the weight is a second-order term. We recall that the linear viscosity term is of second order; thus, the whole nonlinear viscosity term is of fourth-order accuracy. Then, the new nonlinear scheme is of the same order as the fourth-order central

scheme, i.e., we can increase the resolution without loss of accuracy.

3.2. Optimisation of the new scheme

The scheme is now nonlinear; thus, we need to use the nonlinear Fourier analysis method (Li, Leng, and He 2013). This method is primarily designed to analyse the spectral properties of schemes for first derivatives. The analysis of schemes for secondary derivatives can be achieved by simple extension.

Consider a nonlinear finite difference scheme for secondary derivatives, defined as

$$F_j = \Delta x^2 u_j'' = F\left(u_{j-2}, \ldots, u_{j+2}\right) \tag{13}$$

The uniform grids $x_j = j\Delta x$ are given. Let $u_j = \exp(ikx_j)$; then,

$$F_j = (\Delta x)^2 u_j'' = F\left(e^{ik(x_j - p\Delta x)}, \ldots, e^{ik(x_j + q\Delta x)}\right) \tag{14}$$

where p and q are the left and right bounds of the stencil, respectively. We suppose that F_j can be expanded to Fourier space. Then,

$$\begin{aligned} F_j = (\Delta x)^2 u_j'' &= F\left(e^{ik(x_j - p\Delta x)}, \ldots, e^{ik(x_j + q\Delta x)}\right) \\ &= \hat{F}_k e^{ikx_j} \end{aligned} \tag{15}$$

It is known that the exact solution of the difference is

$$F_j^{\text{exact}} = (\Delta x)^2 \left(\frac{\partial^2 u}{\partial x^2}\right)_j = -k^2 (\Delta x)^2 e^{ikx_j} = -\alpha^2 e^{ikx_j} \tag{16}$$

Compared with Equation (15), k_r and k_i for the spectral method are

$$k_r^{\text{exact}} = -\alpha^2, k_i^{\text{exact}} = 0 \tag{17}$$

Thus, the dissipative and dispersive properties of the nonlinear scheme are

$$k_r = k_r(\alpha) = \text{Re}\left(\hat{F}_k\right), k_i = k_i(\alpha) = Im\left(\hat{F}_k\right) \tag{18}$$

We note that for central schemes, k_i is always zero; thus, we only need to analyse k_r. Then, we can use this method to analyse the spectral properties of nonlinear schemes and identify the optimal one. There is an adjustable parameter r in the new scheme. r is optimised to achieve minimum dissipative error. Through optimisation, we obtain the optimal $r = 68/165$. the Fourier property of the optimal scheme (OCD4) is shown in Figure 6, which shows that the dissipative property coincides with the exact solution perfectly at all wave numbers.

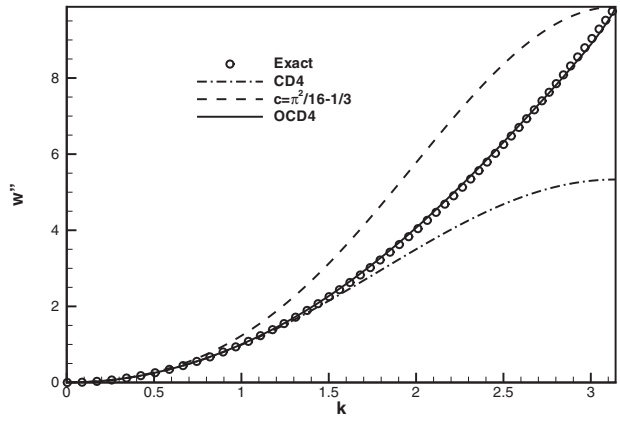

Figure 6. Plot of the Fourier property of schemes with nonlinear optimisation. The solid and dash–dot lines are the reduced wave numbers of OCD4 and CD4, respectively. The dashed line is reduced wave numbers of the linear scheme with c=π^2/16 − 1/3.

Here, we stress that the optimisation is based on the analysis of single cosine/sine waves. For a multi-frequency field, the dissipative property of the new scheme may not be so precise. However, better results can be obtained if we apply the new scheme to practical calculations (see Section 4).

The denominator of the weight may be zero when the scheme is applied to practical simulations. Thus, a small number $\epsilon = 10^{-6}$ is added to the expression of the weight. The final form of the new weight is

$$S_1 = |u_{i+1} + u_{i-1} - 2u_i| + \epsilon \tag{19}$$

$$S_2 = |u_{i+2} + u_{i-2} - 2u_i|/4 + \epsilon \tag{20}$$

$$\hat{\theta}_j = \left|S_1^r - S_2^r\right| / \left|S_1^r + S_2^r\right| \tag{21}$$

where $r = 68/165$. Finally, the expression of OCD4 is as follows:

$$\begin{aligned} \frac{\partial^2 u}{\partial x^2} = &\frac{-(u_{i+2} + u_{i-2}) + 16(u_{i+1} + u_{i-1}) - 30u_i}{12\Delta x^2} \\ &- c_0 \hat{\theta}_j \frac{(u_{i+2} + u_{i-2}) - 4(u_{i+1} + u_{i-1}) + 6u_i}{\Delta x^2} \end{aligned} \tag{22}$$

where $c_0 = \pi^2/16 - 1/3$ and $\hat{\theta}_j$ are defined as Equation (21).

4. Numerical tests

The results of numerical simulations of the simple test cases are presented in the next subsections to assess the performance of the proposed scheme. Most cases were run in under-resolved grid sets to test the ability of the

Table 1 Accuracy comparison of schemes CD4 and OCD4.

Scheme	N	L_∞ error	L_∞ order	L_1 error	L_1 order
CD4	10	44.6485	–	29.7657	–
	20	3.4912	3.6768	2.2251	3.7417
	40	0.2094	4.0594	0.1337	4.0568
	80	1.2728E−002	4.0442	8.1035E−003	4.0443
	160	7.7847E−004	4.0312	4.9566E−004	4.0311
	320	4.8113E−005	4.0161	3.0630E−005	4.0163
OCD4	10	5.1359	–	3.4240	–
	20	0.9372	2.4542	0.5973	2.5192
	40	6.3573E−002	3.8819	4.0571E−002	3.8799
	80	3.9688E−003	4.0016	2.5268E−003	4.0051
	160	2.4430E−004	4.0220	1.5555E−004	4.0219
	320	1.5123E−005	4.0138	9.6276E−006	4.0141

new scheme to suppress unresolved oscillations. As all tests are incompressible cases, there is no need to consider the discretisation of cross-derivatives. We denote the new scheme as OCD4 and the standard fourth-order central scheme as CD4. Note that time integration is performed by means of a standard explicit third-order Runge–Kutta scheme for all calculations hereafter.

4.1. Accuracy test

Supposing that $u = \sin(6\pi x), x \in [0, 1]$, the exact solution of the secondary derivative is $\frac{\partial^2 x}{\partial x^2} = -36\pi^2 \sin(6\pi x)$. Here we do not solve the diffusion equation. Only the order of the secondary derivative is analysed. The convergence tests for the schemes CD4 and OCD4 are shown in Table 1.

The major difference between the two schemes is the resolution at high wave numbers (coarse grid). As seen in Table 1, for a coarse grid, absolute error of OCD4 is one order of magnitude less than that of scheme CD4, although the order of the scheme OCD4 does not reach that of CD4. This property will help dampen spurious oscillations, which are often triggered by under-resolved problems, such as LES or a weak viscous shock. Moreover, as the number of grids increases, the convergence rate approaches that of scheme CD4. Thus, the resolution is increased without accuracy loss when the nonlinear term of OCD4 is written in the current form. We also discover that the absolute error of the new scheme is always less than that of scheme CD4 from the coarsest grid to the finest grid case.

4.2. One-dimensional diffusion equation

The diffusion equation is as follows:

$$\begin{aligned} &\frac{\partial T}{\partial t} = k\frac{\partial^2 T}{\partial x^2}, x \in [0, 1] \\ &T(x, 0) = \sin(6\pi x) \end{aligned} \tag{23}$$

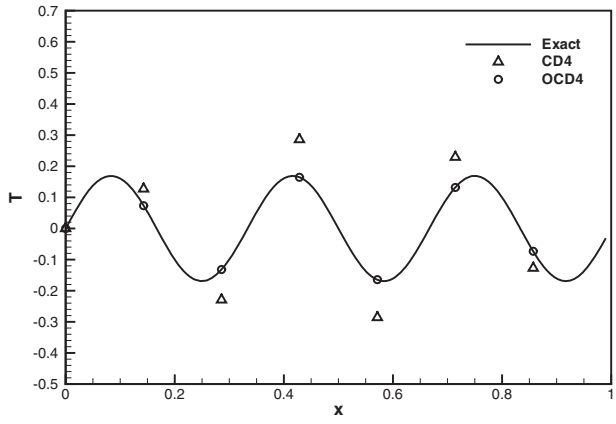

Figure 7. Distribution of T at $t = 5$ for schemes CD4 and OCD4. The solid line is the exact solution. Circles represent the value of the OCD4 and triangles represent the value of CD4.

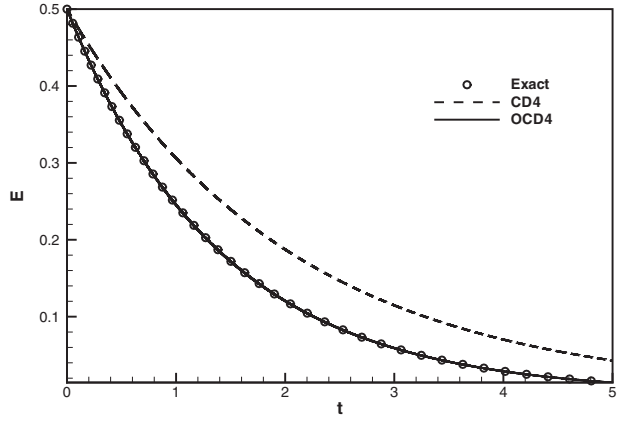

Figure 8. Evolution of E as a function of t for schemes CD4 and OCD4. Circles represent the exact value of energy evolution. The solid and dashed lines represent the energy evolution of CD4 and OCD4, respectively.

where $k = 0.01$. This problem is solved under periodic boundary conditions. We define $E = \int_0^1 T^2 dx$ as the total energy. Figure 7 and 8 display the distribution of T at $t = 5$ and the evolution of E from $t = 0$–5, respectively.

We know that the spectral method is able to capture a sine wave with only two points. This resolution is the limit of the finite difference method. In the current case, there are three waves in the computational domain, which can be resolved by seven points using the spectral method. The problem is solved with eight points to avoid obtaining a trivial solution, and the grid size is 1/7. The numerical results show that the new scheme can capture the exact decaying process of the three waves with only eight points, whereas scheme CD4 deviates substantially from the exact solutions. The resolution of scheme OCD4 is nearly the spectral resolution.

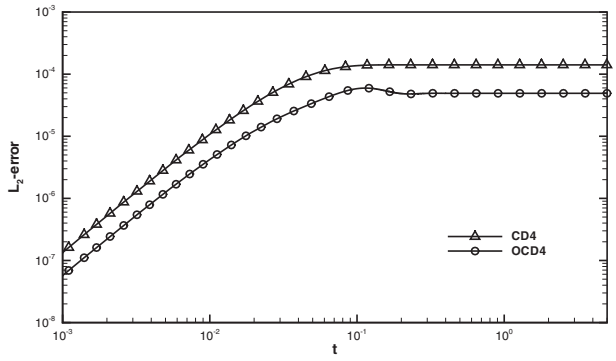

Figure 9. Plot of the evolution of the L_2 error of schemes CD4 and scheme OCD4. The solid line with circles represents the evolution of the L_2 error of scheme OCD4 and the solid line with triangles represents the evolution of the L_2 error of scheme CD4.

4.3. One-dimensional viscous Burger's equation

Next, we address the nonlinear problem with a viscous shock. The 1D viscous Burger's equation is as follows:

$$\frac{\partial u}{\partial t} + u\frac{\partial u}{\partial x} = \frac{1}{\mathrm{Re}}\frac{\partial^2 u}{\partial x^2}, x \in (-1, 1) \tag{24}$$

The analytical solution to the equation is

$$u = -a\tanh\left[\mathrm{Re}\left(0.5ax - ct\right)\right] + c \tag{25}$$

where a and c can be chosen arbitrarily.

In the discretisation of Burgers equation, there are two sources of numerical errors: dispersive errors from the discretisation of the convective terms and dissipative errors from the discretisation of the viscous terms. Because this work is focused on the scheme for the viscous terms (the second derivatives), here we choose a stationary viscous shock with $a = 1$ and $c = 0$ as the test case. As dispersive errors mainly affect the transport speed, dispersive errors can be neglected in stationary cases (Mattsson, Svärd, and Shoeybi 2008).

We set Re = 100 and use 71 points to test the dissipative property of a mildly under-resolved problem (strong shocks require additional artificial dissipation, even in the new scheme). The convective term is written in cannon form (Jameson 2008) and discretised using the fourth-order central scheme, while the viscous term is discretised using schemes CD4 and OCD4. The initial velocity is the exact solution. In Figure 9, we show the convergence histories of different approximations of Burger's equation. It is clear that scheme OCD4 performs as expected. After a long evolution, the L_2-*error* of scheme OCD4 is over one order of magnitude less than that of scheme CD4. The new scheme is more accurate near the shock, as shown in Figure 10, but overshoots after the shock disappears.

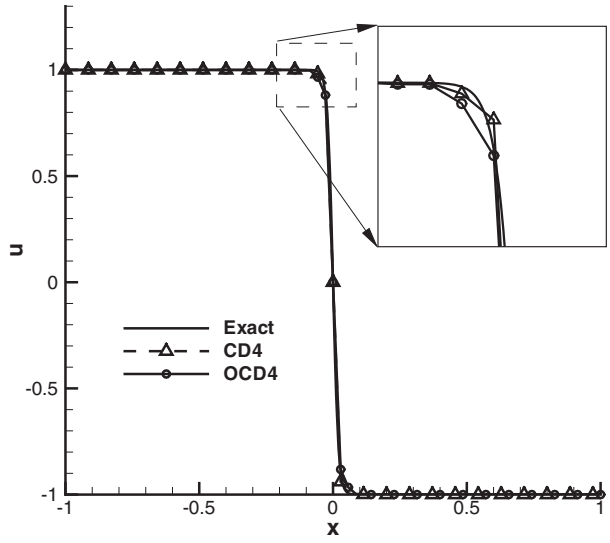

Figure 10. Plot of the distribution of u at $t = 5$ for schemes CD4 and OCD4. The solid line is the exact solution. The solid line with circles represents the value of the OCD4 and the dashed line with triangles represents the value of CD4.

4.4. Two-dimensional vortex decaying

We begin by computing an analytical vortex decaying solution of incompressible Navier–Stokes equations (see Taylor 1923). The initial condition is taken as (Chorin 1968) follows:

$$\begin{aligned} u\left(x, y, 0\right) &= -\cos\left(Nx\right)\sin\left(Ny\right) \\ v\left(x, y, 0\right) &= \sin\left(Nx\right)\cos\left(Ny\right) \\ 0 \le x \le 2\pi, 0 \le y \le 2\pi \end{aligned} \tag{26}$$

The exact solution for this case is known to be

$$\begin{aligned} u\left(x, y, t\right) &= -\cos\left(Nx\right)\sin\left(Ny\right)\exp\left(-2N^2 t/\mathrm{Re}\right) \\ v\left(x, y, 0\right) &= \sin\left(Nx\right)\cos\left(Ny\right)\exp\left(-2N^2 t/\mathrm{Re}\right) \end{aligned} \tag{27}$$

where N is an integer.

This case describes the decaying of an array of vortexes in viscous flow. In the simulation, we set $N = 4$ and Re = 100; the initial vorticity contour is displayed in Figure 11. The convective terms are discretised using the fourth-order central scheme, and the viscous terms are discretised using schemes CD4 and OCD4.

There are four pairs of vortexes in every dimension. We can use a minimum of eight points to capture the decaying process for the scheme with spectral resolution. In our simulation, we use one more point in every dimension to avoid trivial solutions. Here, two sets of grid cells (9^2 and 18^2) are used to test the new scheme.

We also define $E = \int_V (u^2 + v^2)dx/V$; the energy decaying process is as follows.

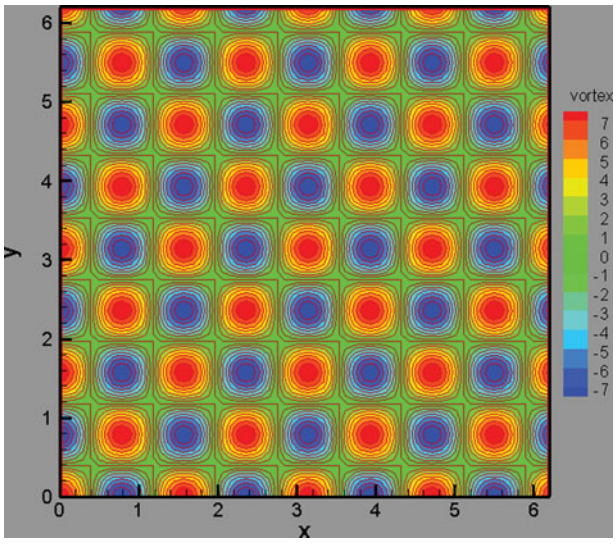

Figure 11. Plot of the initial distribution of u.

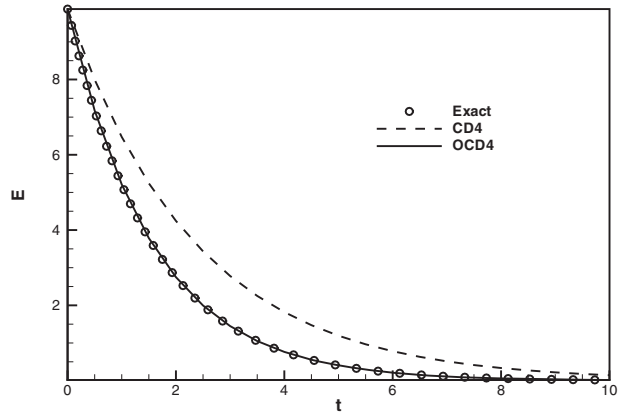

Figure 12. Evolution of E at $N = 9$ for schemes CD4 and OCD4. Circles represent the exact value. The solid and dashed lines are the evolution of total energy with schemes OCD4 and CD4, respectively.

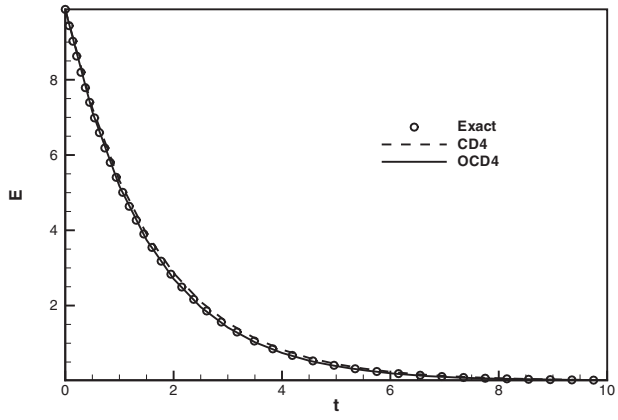

Figure 13. Evolution of E at $N = 18$ for schemes CD4 and OCD4. Circles represent the exact value. The solid and dashed lines are the evolution of total energy with schemes OCD4 and CD4, respectively.

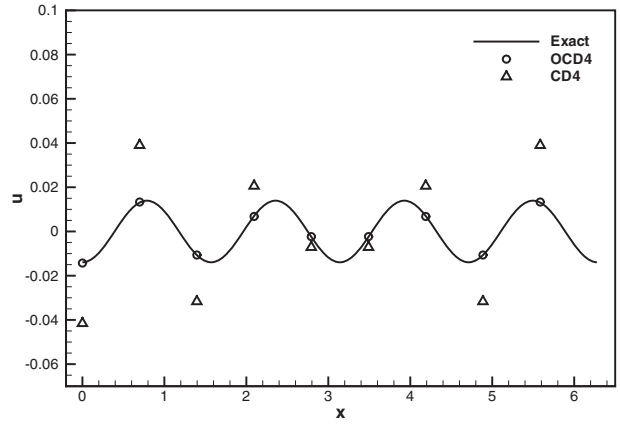

Figure 14. Plot of the distribution of u at $y = 2\pi/9$ for schemes CD4 and OCD4. The solid line represents the exact value. Circles represent results with scheme OCD4 and triangles represent results with scheme CD4.

Figure 12 and 13 show the evolution of E for grids 9^2 and 18^2, respectively. Even if a grid of 9^2 is used, the decaying process can be exactly captured by the new scheme. The resolution of the new scheme is as high as that of the spectral method. In Figure 14, the distribution of u at $y = 2\pi/9$ confirms this property. Because of the dissipation deficiency of scheme CD4, after a long evolution, the relative error at an extreme point may exceed 100%, and scheme CD4 fails to catch the decay process. In contrast, the results of OCD4 are almost the same as the exact value.

4.5. Three-dimensional incompressible isotropic homogeneous turbulence

Now, we consider the 3D incompressible Navier–Stokes equations. The first case is homogeneous decaying isotropic turbulence, which is simulated in a cubic box of length 2π. As suggested by Samtaney, Pullin, and Kosovic (2001), the initial energy spectrum is $E(k) = Ak^4 e^{-2k^2/k_0^2}$, and $k_0 = 8$ and $A = 0.00013$ are chosen. The initial Re_λ is 58, and the turnover time is $\tau = \sqrt{\frac{32}{A}(2\pi)^{1/4} k_0^{-7/2}}$.

We aimed to test the behaviour of the new scheme for coarse grids. In this case, both convective terms and viscous terms exert great influence on small scales. To eliminate the errors caused by convective terms, we treat convective terms with the spectral method and use the 3/2 rule to remove aliasing errors. The viscous terms are discretised by using schemes CD4, OCD4 and the spectral method. We choose the grids 32^3 and 128^3 to test the new scheme. The two sets of grids refer to LES and DNS grids, respectively. No subgrid-scale (SGS) model is added to test the effect of the schemes alone. Figure 15 and 16 display the resolved turbulent energy decaying processes of

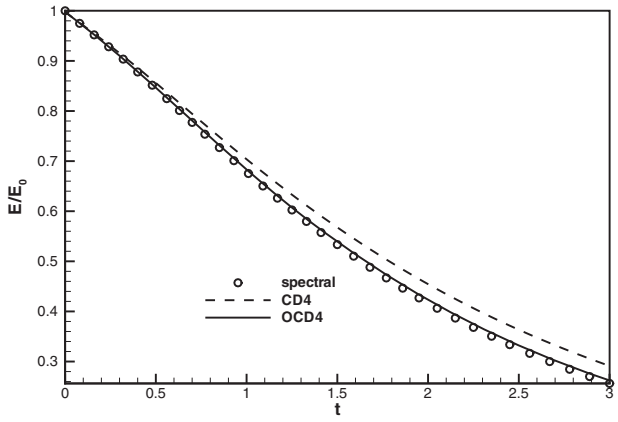

Figure 15. Plots of the evolution of E at $N = 32$ for schemes CD4 and OCD4. Circles represent the results with spectral method. The solid and dashed lines are the evolution of total energy with schemes OCD4 and CD4, respectively.

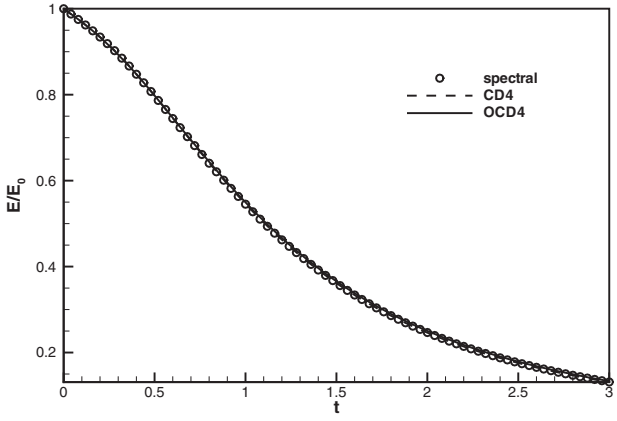

Figure 16. Plots of the evolution of E at $N = 128$ for schemes CD4 and OCD4. Circles represent the results with spectral method. The solid and dashed lines are the evolution of total energy with schemes OCD4 and CD4, respectively.

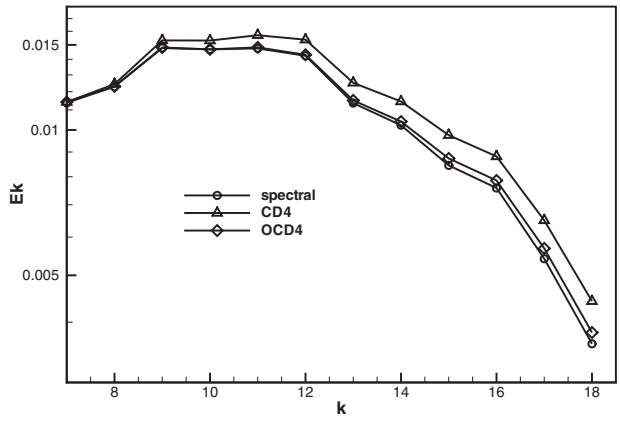

Figure 17. Plots of the energy spectrum at $t = 1.5$ for schemes CD4 and OCD4. The solid line with circles represents the result of spectral method. The solid line with diamonds represents the results with scheme OCD4. The solid line with triangles represents the results with scheme CD4.

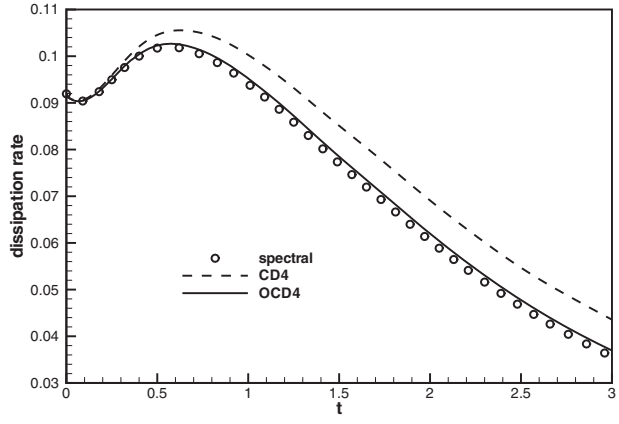

Figure 18. Plots of the evolution of the dissipation rate at $N = 32^3$ for schemes CD4 and OCD4. Circles represent the results with spectral method. The solid and dashed lines are the results with schemes OCD4 and CD4, respectively.

different grids ($N = 32^3$ and $N = 128^3$). The resolved total turbulent energy is defined as $E = \frac{1}{2}\langle u_i u_i \rangle$, where the angle brackets represent the spatial average.

At $N = 32^3$, scheme CD4 greatly overestimates the turbulent energy, whereas the result of scheme OCD4 agrees well with the spectral method. This is because the decaying of turbulent energy is mainly attributable to the viscous dissipation at high wave numbers, and scheme CD4 severely underestimates this dissipation. At $N = 128^3$, where the resolution is sufficient, the results of both schemes coincide with that of the spectral method.

Figure 17 and 18 show the resolved energy spectrum at $t = 1.5$ and the evolution of the dissipation rate at $N = 32^3$. Scheme CD4 overestimates the energy spectrum at high wave numbers for coarse grids, whereas the new scheme can suppress the excess energy, which allows its results to agree well with those of the spectral method. Similarly, the dissipation rate results are more accurate when using the new scheme. The above results show that the numerical errors of scheme CD4 cannot be neglected for coarse grids. This conclusion indicates that we must use high-resolution schemes in LES instead of scheme CD4.

The improvement of the skewness of velocity derivatives provides further evidence of the advantages of the new scheme. Figure 19 shows the skewness of $\partial u/\partial x$ at $N = 128^3$. The skewness obtained using scheme OCD4 coincides with that of the spectral method, while scheme CD4 overestimates the skewness, even for fine grids (DNS grids). Thus, we draw the same conclusion as that of Suzuki et al. (2013): using high-resolution schemes for viscous terms will improve the accuracy of high-order statistics in DNS.

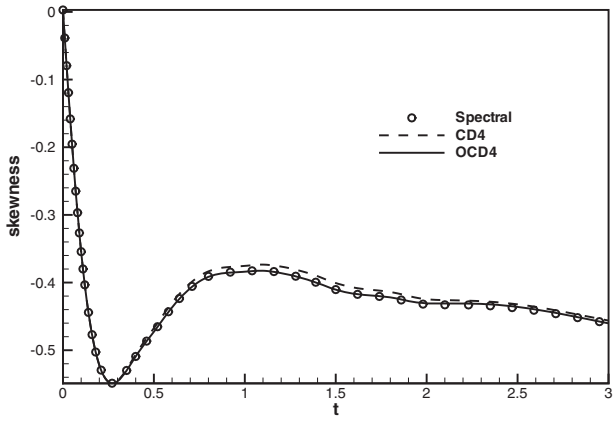

Figure 19. Plots of skewness at $N = 128^3$ for schemes CD4 and OCD4. Circles represent the results with spectral method. The solid and dashed lines are the results with schemes OCD4 and CD4, respectively.

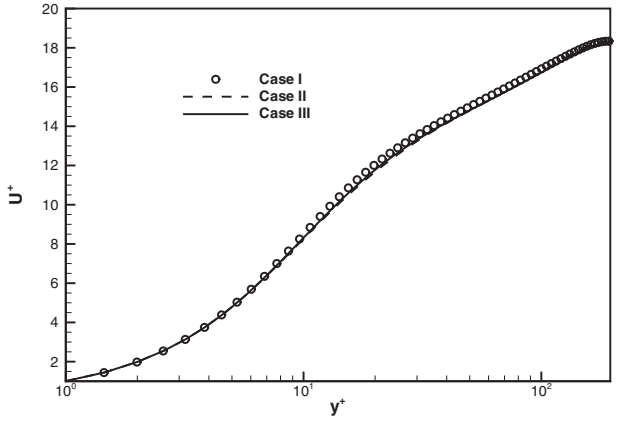

Figure 20. Plots of mean stream-wise velocity profiles for schemes CD4 and OCD4. Circles represent the stream-wise velocity profile of case I. The solid line represents the streamwise velocity profile of case II with scheme OCD4. The dashed line represents the streamwise velocity profile of case III with scheme CD4.

4.6. Incompressible turbulent channel flow

The second 3D case is incompressible turbulent channel flow. The channel flow is initialised by a laminar flow (Poiseuille profile) with random disturbance with amplitudes of approximately 1% of the streamwise velocity. Periodic boundary conditions are applied in the streamwise (x) and spanwise (z) directions, and the volume force that drives the flow is adjusted dynamically to maintain a constant mass flux through the channel. The friction Reynolds number, which is based on the wall friction velocity, u_τ, and the channel half height δ, is $\mathrm{Re}_\tau = 191$. Two sets of grids (96*129*96 and 192*129*192) are calculated. The resolution of the fine grid is suitable for DNS, and that of the coarse grid is slightly under-resolved. For the coarse grid, no SGS model is used to compare the effects of the schemes. The case of the fine grids is named

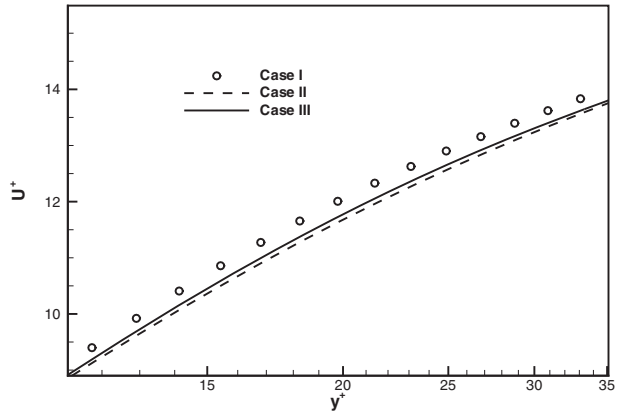

Figure 21. Partial view of mean streamwise velocity profiles near buffer layer region for schemes CD4 and OCD4. Circles represent the streamwise velocity profile of case I. The solid line represents the streamwise velocity profile of case II with scheme OCD4. The dashed line represents the streamwise velocity profile of case III with scheme CD4.

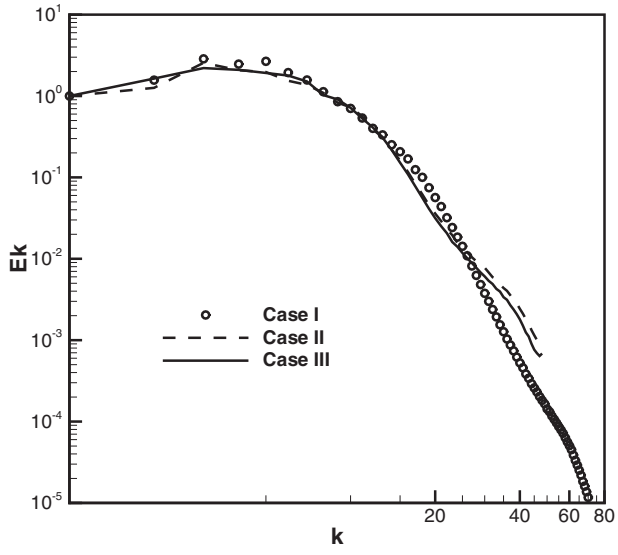

Figure 22. Plots of the energy spectra of streamwise velocity for schemes CD4 and OCD4. Circles represent the energy spectra of streamwise velocity of case I. The solid line represents the energy spectra of streamwise velocity of case II with scheme OCD4. The dashed line represents the energy spectra of streamwise velocity of case III with scheme CD4.

case I. The cases with coarse grids are named case II and case III for schemes CD4 and OCD4, respectively.

The mean value of three velocity components are averaged in time and over horizontal planes. Figure 20 shows the mean streamwise velocity profiles for the three cases. There is not much difference among the mean velocities of case I, case II and case III. The partial enlarged view of the buffer layer region in Figure 21 shows that scheme OCD4 performs better in the buffer layer region. The energy spectra of streamwise, spanwise and vertical velocities are displayed in Figure 22–24. The energy

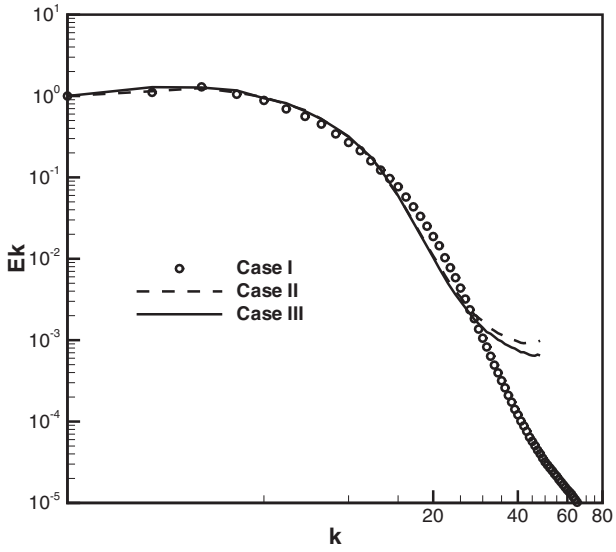

Figure 23. Plots of the energy spectra of spanwise velocity for schemes CD4 and OCD4. Circles represent the energy spectra of spanwise velocity of case I. The solid line represents the energy spectra of spanwise velocity of case II with scheme OCD4. The dashed line represents the energy spectra of spanwise velocity of case III with scheme CD4.

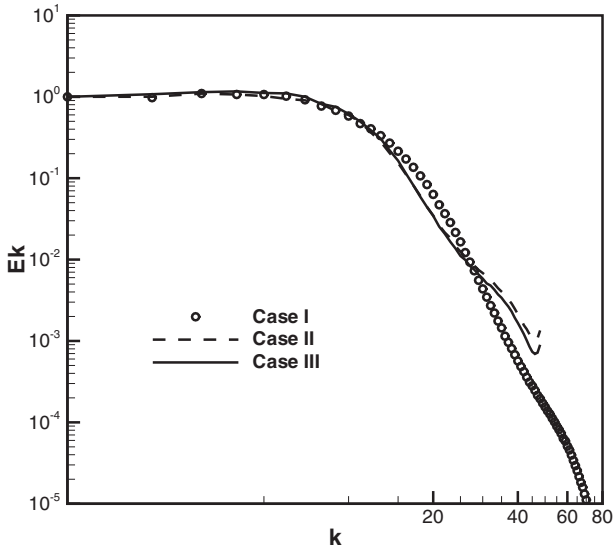

Figure 24. Plots of the energy spectra of vertical velocity for schemes CD4 and OCD4. Circles represent the energy spectra of vertical velocity of case I. The solid line represents the energy spectra of vertical velocity of case II with scheme OCD4. The dashed line represents the energy spectra of vertical velocity of case III with scheme CD4.

spectra of the velocities calculated using scheme CD4 are larger than those calculated using scheme OCD4 within a high wave number range, showing that scheme CD4 overestimates the energy at all scales. The additional dissipation in scheme OCD4 can dampen the extra energy and improve the results. Similar but larger differences in energy spectra for high-order statistics are observed

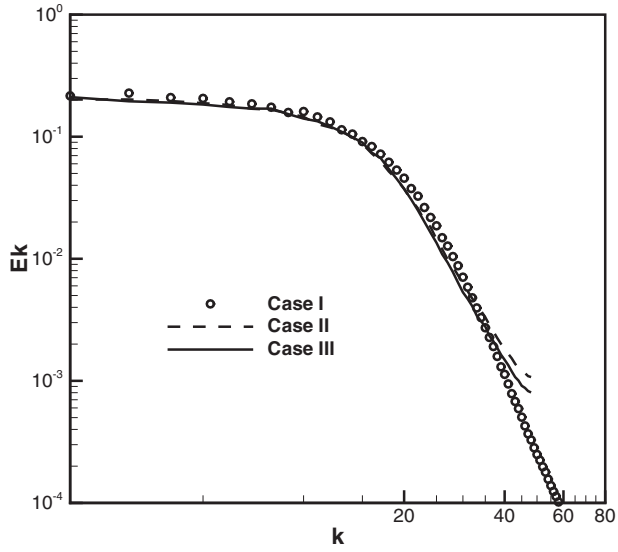

Figure 25. Plots of the energy spectra of Reynolds stress for schemes CD4 and OCD4. Circles represent the energy spectra of Reynolds stress of case I. The solid line represents the energy spectra of Reynolds stress of case II with scheme OCD4. The dashed line represents the energy spectra of Reynolds stress of case III with scheme CD4.

in Figure 25, which presents spectra of the Reynolds stresses.

5. Summary and conclusion

A new nonlinear scheme for secondary derivatives with a 5-point stencil is proposed to increase both the resolution and stability of schemes for secondary derivatives. The dissipative property of the new scheme coincides with the spectral method over the whole wave number range. The new scheme is a combination of a fourth-order central scheme and an artificial viscosity term. These two parts are connected by a nonlinear weight, which was designed specifically for the smooth region. The proposed nonlinear weight is independent of physical positions for a cosine wave at a certain wave number, which is important for optimisation in Fourier space. Nonlinear Fourier analysis is performed to optimise the new scheme to achieve spectral-like resolution over the whole wave number range. An accuracy test shows that the resolution is increased without accuracy loss.

Five cases (diffusion equation, Burger's equation, vortex decay problem, isotropic homogeneous turbulence and fully developed turbulent channel flow) verify the spectral properties of the new scheme. The diffusion equation and vortex decaying problem reveal that the new scheme can capture the evolution of energy using the same grid as the spectral method. The results of the steady Burger's problem show that the new scheme can

smear the overshoot near a steady viscous shock. In the case of the decaying homogeneous isotropic turbulence problem, the advantage of the new scheme is more evident in coarse grids. The new scheme can dampen spurious energy accumulation at high wave numbers. The energy evolution and dissipation rate calculated using the new scheme are more accurate than those of scheme CD4. The skewness results indicate that the new scheme can improve the accuracy of high-order statistics, as demonstrated by Suzuki et al. (2013).

Acknowledgements

Thanks to Profs. Dexun Fu and Yanwen Ma from the Institute of Mechanics, CAS, for their help. This work is supported by NSFC Projects (Nos. 1372330, 11472278, 11472010), the 863 Program (No. 2012AA01A304) and the CAS Program (KJCX2-EW-J01, XXH12503-02-02-04). The authors thank the National Supercomputer Center in Tianjin (NSCC), the Supercomputing Center of the Chinese Academy of Sciences (SCCAS) and the Shangdong Supercomputing Center for providing computer time.

Disclosure statement

No potential conflict of interest was reported by the authors.

Funding

This work is supported by National Natural Science Foundation of China Projects [grant number 1372330], [grant number 11472278], [grant number 11472010]; the National HighTechnology Research and Development Program of China [grant number 2012AA01A304]; the Chinese Academy of Sciences Program [grant number KJCX2-530 EW-J01], [grant number XXH12503-02-02-04].

References

Borges, Rafael, Monique Carmona, Bruno Costa, and Wai Sun Don. 2008. "An Improved Weighted Essentially Non-oscillatory Scheme for Hyperbolic Conservation Laws." *Journal of Computational Physics* 227 (6): 3191–3211.

Chorin, Alexandre J. 1968. "Numerical Solution of the Navier–Stokes Equations." *Mathematics of Computation* 22 (104): 745–762.

Chow, Fotini K, and Parviz Moin. 2003. "A Further Study of Numerical Errors in Large-Eddy Simulations." *Journal of Computational Physics* 184 (2): 366–380.

De, Arnab K, and Vinayak Eswaran. 2006. "Analysis of a New High Resolution Upwind Compact Scheme." *Journal of Computational Physics* 218 (1): 398–416.

Deng, Xiaogang, Meiliang Mao, Guohua Tu, Hanxin Zhang, and Yifeng Zhang. 2012. "High-Order and High Accurate CFD Methods and Their Applications for Complex Grid Problems." *Communications in Computational Physics* 11 (4): 1081.

Deng, Xiaogang, and Hanxin Zhang. 2000. "Developing High-Order Weighted Compact Nonlinear Schemes." *Journal of Computational Physics* 165 (1): 22–44.

Ducros, F, V. Ferrand, F. Nicoud, C. Weber, D. Darracq, C. Gacherieu, and T. Poinsot. 1999. "Large-Eddy Simulation of the Shock/Turbulence Interaction." *Journal of Computational Physics* 152 (2): 517–549.

Fu, Dexun, and Yanwen Ma. 1997. "A High Order Accurate Difference Scheme for Complex Flow Fields." *Journal of Computational physics* 134 (1): 1–15.

Gerolymos, G. A, and I. Vallet. 2012. "Very-High-Order Conservative Discretization of Diffusive Terms with Variable Viscosity." Paper presented at Seventh International Conference on Computational Fluid Dynamics, Big Island, Hawaii, July 9–13.

Harten, Amiram. 1978. "The Artificial Compression Method for Computation of Shocks and Contact Discontinuities. III. Self-adjusting Hybrid Schemes." *Mathematics of Computation* 32 (142): 363–389.

Jameson, Antony. 2008. "The Construction of Discretely Conservative Finite Volume Schemes That Also Globally Conserve Energy or Entropy." *Journal of Scientific Computing* 34 (2): 152–187.

Jameson, Antony, Wolfgang Schmidt, and Eli Turkel. 1981. "Numerical solution of the Euler equations by finite volume methods using Runge Kutta time stepping schemes." Paper presented at AIAA, Fluid and Plasma Dynamics Conference, 14th, Palo Alto, CA, June 23–25.

Jiang, Guang-Shan, and Chi-Wang Shu. 1996. "Efficient Implementation of Weighted ENO Schemes." *Journal of Computational Physics* 126 (1): 202–228.

Kennedy, Christopher A., and Andrea Gruber. 2008. "Reduced Aliasing Formulations of the Convective Terms within the Navier–Stokes Equations for a Compressible Fluid." *Journal of Computational Physics* 227 (3): 1676–1700.

Lele, Sanjiva K. 1992. "Compact Finite Difference Schemes with Spectral-Like Resolution." *Journal of Computational Physics* 103 (1): 16–42.

Li, Xinliang, Dexun Fu, and Yanwen Ma. 2010. "Direct Numerical Simulation of Hypersonic Boundary Layer Transition Over a Blunt Cone with a Small Angle of Attack." *Physics of Fluids (1994-present)* 22 (2): 025105.

Li, Xin-liang, Yan Leng, and Zhi-Wei He. 2013. "Optimized Sixth-Order Monotonicity-Preserving Scheme by Nonlinear Spectral Analysis." *International Journal for Numerical Methods in Fluids* 73 (6): 560–577.

Liang, Xian, Xinliang Li, Dexun Fu, and Yanwen Ma. 2009. "Complex Transition of Double-Diffusive Convection in a Rectangular Enclosure with Height- to-Length Ratio Equal to 4: Part I." *Communications in Computational Physics* 6 (2): 247.

Martín, M. P., E. M. Taylor, M. Wu, and V. G. Weirs. 2006. "A Bandwidth-Optimized WENO Scheme for the Effective Direct Numerical Simulation of Compressible Turbulence." *Journal of Computational Physics* 220 (1): 270–289.

Mattsson, Ken. 2012. "Summation by Parts Operators for Finite Difference Approximations of Second-Derivatives with Variable Coefficients." *Journal of Scientific Computing* 51 (3): 650–682.

Mattsson, Ken, Magnus Svärd, and Mohammad Shoeybi. 2008. "Stable and Accurate Schemes for the Compressible Navier–Stokes Equations." *Journal of Computational Physics* 227 (4): 2293–2316.

Mohammadian, A. 2010. "Numerical Approximation of Viscous Terms in Finite Volume Models for Shallow Waters." *International Journal for Numerical Methods in Fluids* 63 (5): 584–599.

Nagarajan, Santhanam, Sanjiva K. Lele, and Joel H. Ferziger. 2003. "A Robust High-Order Compact Method for Large Eddy Simulation." *Journal of Computational Physics* 191 (2): 392–419.

Pirozzoli, Sergio. 2011. "Numerical Methods for High-Speed Flows." *Annual Review of Fluid Mechanics* 43: 163–194.

Qin, Q., Z. A. Xia, and Z. F. Tian. 2014. "High Accuracy Numerical Investigation of Double-Diffusive Convection in a Rectangular Enclosure with Horizontal Temperature and Concentration Gradients." *International Journal of Heat and Mass Transfer* 71: 405–423.

Ren, Yu-Xin, Miao'er Liu, and Hanxin Zhang. 2003. "A Characteristic-Wise Hybrid Compact-WENO Scheme for Solving Hyperbolic Conservation Laws." *Journal of Computational Physics* 192 (2): 365–386.

Samtaney, R., D. I. Pullin, and B. Kosovic. 2001. "Direct Numerical Simulation of Decaying Compressible Turbulence and Shocklet Statistics." *Physics of Fluids* 13 (5): 1415–1430.

Sayadi, Taraneh, and Parviz Moin. 2012. "Large Eddy Simulation of Controlled Transition to Turbulence." *Physics of Fluids (1994-present)* 24 (11): 114103.

Shen, Yiqing, and Gecheng Zha. 2010. "Large Eddy Simulation Using a New Set of Sixth Order Schemes for Compressible Viscous Terms." *Journal of Computational Physics* 229 (22): 8296–8312.

Shen, Yiqing, Gecheng Zha, and Xiangying Chen. 2009. "High Order Conservative Differencing for Viscous Terms and the Application to Vortex-Induced Vibration Flows." *Journal of Computational Physics* 228 (22): 8283–8300.

Suzuki, H., K. Nagata, Y. Sakai, T. Hayase, Y. Hasegawa, and T. Ushijima. 2013. "An Attempt to Improve Accuracy of Higher-Order Statistics and Spectra in Direct Numerical Simulation of Incompressible Wall Turbulence by Using the Compact Schemes for Viscous Terms." *International Journal for Numerical Methods in Fluids* 73 (6): 509–522.

Taylor, G. I. 1923. "LXXV. On the Decay of Vortices in a Viscous Fluid." *The London, Edinburgh, and Dublin Philosophical Magazine and Journal of Science* 46 (274): 671–674.

Tian, Zhenfu, Xian Liang, and Peixiang Yu. 2011. "A Higher Order Compact Finite Difference Algorithm for Solving the Incompressible Navier–Stokes Equations." *International Journal for Numerical Methods in Engineering* 88 (6): 511–532.

Tian, Zhen F., and P. X. Yu. 2011. "An Efficient Compact Difference Scheme for Solving the Stream Function Formulation of the Incompressible Navier–Stokes Equations." *Journal of Computational Physics* 230 (17): 6404–6419.

Tu, Guo-Hua, Xiao-Gang Deng, and Mei-Liang Mao. 2011. "A Staggered Non-oscillatory Finite Difference Method for High-Order Discretization of Viscous Terms." *Acta Aerodynamica Sinica* 29 (1): 10–15.

Vaassen, J-M, D Vigneron, and J-A Essers. 2008. "An Implicit High Order Finite Volume Scheme for the Solution of 3D Navier–Stokes Equations with New Discretization of Diffusive Terms." *Journal of Computational and Applied Mathematics* 215 (2): 595–601.

Yanwen, Ma, Fu Dexun, T. Kobayashi, and N. Taniguchi. 1999. "Numerical Solution of the Incompressible Navier–Stokes Equations with an Upwind Compact Difference Scheme." *International Journal for Numerical Methods in Fluids* 30 (5): 509–521.

Yu, Changping, Renkai Hong, Zuoli Xiao, and Shiyi Chen. 2013. "Subgrid-Scale Eddy Viscosity Model for Helical Turbulence." *Physics of Fluids (1994-present)* 25 (9): 095101.

Zingg, D. W., S. De Rango, M. Nemec, and T. H. Pulliam. 2000. "Comparison of Several Spatial Discretizations for the Navier–Stokes Equations." *Journal of Computational Physics* 160 (2): 683–704.